Available online at www.sciencedirect.com
SCIENCE DIRECT®
International Journal of Heat and Mass Transfer 49 (2006) 825–835
International Journal of HEAT and MASS TRANSFER
www.elsevier.com/locate/ijhmt

Experimental and theoretical temperature distributions in a solar pond

M. Karakilcik [a], K. Kıymaç [a], I. Dincer [b,*]

[a] Department of Physics, Faculty of Sciences and Letters, University of Çukurova, Adana 01330, Turkey
[b] Faculty of Engineering and Applied Science, University of Ontario Institute of Technology (UOIT), 2000 Simcoe Street North, Oshawa, Ont., Canada L1H 7K4

Received 24 November 2004
Available online 28 November 2005

Abstract

In this study, an experimental and theoretical investigation of temperature distributions in an insulated solar pond, particularly during daytimes and nighttimes, is presented. Several temperature sensors connected to a data acquisition are placed vertically inside and the bottom of the pond and also horizontally and vertically in the insulated side walls, and used to measure temperature changes with time and position. In addition, we model the solar pond to compute theoretical temperature distributions and compare with the experimental measurements, and hence a good agreement is found between experimental and theoretical temperature profiles. There is a large amount of heat losses between daytimes and nighttimes, depending upon the temperature difference, and these present a significant potential for energy savings and storage. During the months of January, May and August, it is found that the total heat losses from the inner surface of the pond and its bottom and side walls, as a function of temperature difference, are determined to account for 227.76 MJ (e.g., 84.94% from the inner surface, 3.93% from the bottom and 11.13% from the side walls, respectively).
© 2005 Elsevier Ltd. All rights reserved.

Keywords: Heat transfer; Temperature distribution; Heat storage; Heat losses; Solar pond

1. Introduction

A salinity gradient solar pond is an integral collection and storage device of solar energy. By virtue of having built-in thermal energy storage, it can be used irrespective of time and season. In an ordinary pond or lake, when the sun's rays heat up the water this heated water, being lighter, rises to the surface and loses its heat to the atmosphere. The net result is that the pond water remains at nearly atmospheric temperature. The solar pond technology inhibits this phenomenon by dissolving salt into the bottom layer of this pond, making it too heavy to rise to the surface, even when hot. The salt concentration increases with depth, thereby forming a salinity gradient. The sunlight, which reaches the bottom of the pond, remains entrapped there. The useful thermal energy is then withdrawn from the solar pond in the form of hot brine. The pre-requisites for establishing solar ponds are: a large tract of land (it could be barren), a lot of sunshine, and cheaply available salt (e.g., NaCl) or bittern. Solar ponds were pioneered in the early 1960s, and are simple in principle and operation. They are long-lived and require little maintenance. Heat collection and storage are accomplished in the same unit, as in passive solar structures, and the pumps and piping used to maintain the salt gradient are relatively simple. The ponds need cleaning, like a swimming pool, to keep the water transparent to light. A major advantage of solar ponds is the independence of the system. No backup is needed because the pond's high heat capacity and enormous thermal mass can usually buffer a drop in

* Corresponding author. Tel.: +1 905 721 3209x2573; fax: +1 905 721 3140.
E-mail addresses: kkilcik@cu.edu.tr (M. Karakilcik), kiymac@cu.edu.tr (K. Kıymaç), ibrahim.dincer@uoit.ca (I. Dincer).

0017-9310/$ - see front matter © 2005 Elsevier Ltd. All rights reserved.
doi:10.1016/j.ijheatmasstransfer.2005.09.026

Nomenclature

A	surface area (m^2)
C	the specific heat (J/kg °C)
E	total solar energy reaching pond (J)
F	absorbed energy fraction at a region of δ-thickness
h	solar radiation ratio given in Eq. (4)
HSZ	heat storage zone
I	number of layers
IB	insulated bottom wall
ISW	insulated side walls
IZ	insulation zone
J	column number of the cells
K	$1,2,3,\ldots,24$ (index for time interval Δt)
k	thermal conductivity (J/kg °C h)
LCZ	lower convective zone
NCZ	non-convective zone
Q	heat (J)
R	thermal resistance of the side walls (°C h/J)
S	thickness (mm)
T	temperature (°C)
U	heat transfer coefficient between the ambient air and solar pond (hourly basis) (MJ/m^2 °C h)
UCZ	upper convective zone
X	thickness of inner zones (m)

Greek symbols

δ	thickness where long-wave solar energy is absorbed (m)
β	incident beam entering rate into water
θ	angle (rad)
ρ	density (kg/m^3)
Δx	thickness of horizontal layers (mm)
Δy	thickness of vertical layers (mm)
Δt	time difference (h)

Subscripts

amb	ambient
b	bottom
down	just below zone
dy	day
i	incident
in	to reach net irradiation solar energy of zone
ins	insulator
j	column number
ls	heat loss
L	length
n	number of day (1–365)
net	net solar irradiation
ng	night
p	paint
ps	painted metal sheet for first layer
r	reflection
s	sheet-iron
side	side wall
solar	solar irradiation inner zones of pond
stored	stored energy inner zones of pond
up	just above zone
w	width
wa	from water to air
01	first ring inner surface surrounding pond

solar supply that would force a single-dwelling unit to resort to backup heat [1].

Recently, there has been increasing interest in environmentally benign and sustainable energy sources, e.g., solar energy. In this regard, solar ponds receive some increasing attention for implementation. In the open literature, numerous experimental and theoretical studies have been undertaken by various researchers (e.g., [2–19]). Experimental works (e.g., [3–12]) basically concentrate on design, application and experimental thermal measurements in solar ponds to investigate the thermal behavior of various types of solar ponds in different dimensions. Theoretical studies (e.g., [2,12–19]) are particularly focused on modeling of solar ponds for their performance analysis, predicting temperature variations in the ponds, and developing empirical correlations as a function of air and soil temperatures. Solar energy is absorbed by a solar pond from its surroundings during the day and stored in the form of heat energy in it. During the nights, due to non-existence of solar energy, no contribution is made to the pond's thermal energy. To the best of authors' knowledge, there have not been experimental and theoretical studies investigating heat losses from the inner zones and side walls of the solar ponds during daytimes and nighttimes and comparing both experimental and theoretical temperature variations. This is essentially the aim of the present paper.

2. Experimental apparatus and procedure

In general, solar ponds are composed of three zones as follows:

- The first zone, upper convective zone (UCZ), is the fresh water layer at the top of the pond. This zone is fed with fresh water in order to maintain its density as close as to the density of fresh water in the upper part and meet the lost water due to evaporation.
- The second (middle) zone is the insulation zone (IZ) between the lower convective zone (LCZ) and the UCZ. The IZ (so-called non-convective zone (NCZ)) is composed of salty water layers whose brine density gradually increases towards LCZ. NCZ is the key to the working of a solar pond. It allows solar an extensive amount of work on solar pond as a radiation to pene-

trate into the storage zone while cost-effective method of collecting and storing prohibiting the propagation of long wave radiation solar energy on large scale is available in the because water is opaque to infrared radiation.

- The third zone is known as the lower convective zone (LCZ) (so-called as the heat storage zone (HSZ)) and is composed of salty water with highest density. Considerable part of the solar energy is absorbed and stored by this bottom region. LCZ has the highest temperature, and hence, the strongest thermal interaction occurs between this zone and the insulated bottom wall (IBW) and insulated side walls (ISW) surrounding it.

For the experimental works, a solar pond with a surface area of 2 m × 2 m, and a depth of 1.5 m was built in Cukurova University in Adana, Turkey and used to measure temperature variations during daytime and nighttime at the bottom and side walls of the pond. The bottom and the side walls of the pond were plated with the iron-sheets in 5 mm thickness, and in between with a glass-wool of 50 mm thickness as the insulating layer. It was built on the iron steel base to 0.5 m height from the ground and insulated by 20 mm wood slats thickness from the iron steel base. Inner and out sides of the pond were painted with anti-corrosion paint to avoid corrosion. Fig. 1 illustrates the inner zones of the solar pond and the measurement points. Inner zones consist of the salty water layers with various densities. The experimental temperature distributions were measured using 16 heat sensors, which were placed into the inner zones and the insulated walls of the pond. Hence the temperature distribution profiles of these regions at any time were experimentally obtained by a data acquisition system [19]. To measure the temperature distributions of various regions, the temperature sensors were placed into the inner zones, starting from the bottom, at 0.05, 0.30, 0.55, 0.70, 0.80, 1.05, 1.35, 1.50 m heights, from the bottom downwards into the insulated bottom, at 15 and 45 mm and into the side walls, starting from the bottom to 0, 0.35, 0.65, 0.75, 1.00, 1.35 m heights. The data acquisition system was connected to a computer for data recording, monitoring and processing. The inner and wall

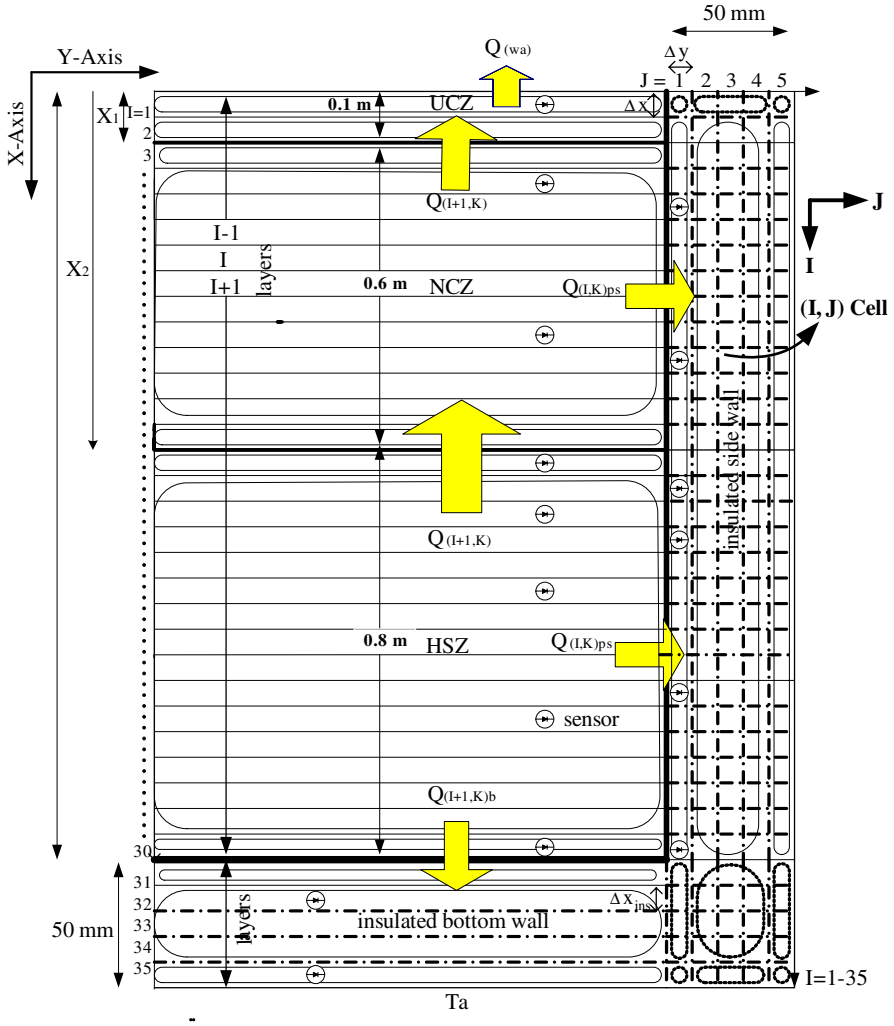

Fig. 1. Schematics of the insulated solar pond and the temperature measurement points.

Table 1
Thermophysical properties of materials

	Water	Salina water	Painted wall	Insulation	Air
Density (kg/m^3)	998	1185	7849	200	1.16
Thermal conductivity (J/m K h)	2160	–	21200	143	94.68
Specific heat (J/kg K)	4182	–	460	670	1007

Source: [1,19].

temperatures of the pond were measured on hourly basis throughout day and night. The temperatures at the inner zones and insulated side wall of the pond were measured by the sensors with a range of −65 to +155 °C, and with a measurement accuracy of ±0.1 °C for the temperature range of 0–120 °C. The sensors consisted of 1N4148 semiconductor devices with coaxial cables in different lengths between 17 and 20 m. The solar energy data obtained by using a pyranometer, and hourly average air and daily average insulator temperatures taken from a local meteorological data as input parameters for the modeling part below were used. Thus, Table 1 gives some thermophysical properties of materials used in the model.

In addition to the temperature measurements, a theoretical modeling is proposed to estimate the temperature distributions at the bottom layer and side walls and compared with the measurements carried out during the experiments. Note that in the model, solar energy (Q_{solar}), is taken as $Q_{\text{solar}} > 0$ to sunset from sunrise for daytime, and $Q_{\text{solar}} = 0$ to sunrise from sunset for the night for a day.

3. Modeling

In order to understand the thermal behavior of the solar pond, the temperature distributions of its regions should be determined. To realize this, the pond is separated into two essential regions, the inside and the outside parts. The inside of the pond is UCZ, NCZ, HSZ and the insulated bottom wall, and the outside of it is the insulated side walls. The temperature variations of these two sections depend on the solar energy that reaches on the horizontal surface, the climate conditions of the place, the structure of the pond, time, and the insulation specifications. The structure of the pond should be known when the temperature distribution is calculated, a cross-section of it is shown in Fig. 1. The inner section of the model pond is divided into 30 imaginary layers with a thickness $\Delta x = 50$ mm and the insulated bottom wall is divided into 5 imaginary layers each of thickness $\Delta x_{\text{ins}} = 10$ mm. Basically, the heat balance equations are written in one-dimensional for UCZ, NCZ, HSZ and the bottom wall to determine the temperature distributions of these regions. But, for the insulated side walls one needs two-dimensional heat balance equation as outlined earlier [14]. Hence, the outside region is divided into small imaginary cells of masses by separating it into vertical layers of thickness $\Delta y = 10$ mm and horizontal layers of thickness 50 mm. Two-dimensional heat balance equations are written down for each cellular mass, which are presented towards the end of this section. Both one and two-dimensional heat balance equations are written in the finite difference form for the brine and for the insulation surrounding the pond in the following sections, respectively. The present model is a modified version of the one developed by Kayalı et al. [14] which was a function of soil temperature and considered the heat storage zone one layer only. Some of the unique characteristics of this model are the variable surface area, as a function of air temperature rather than soil temperature, and a multiple layered heat storage zone.

Here we write the general energy balance equation for the solar pond in the following form:

$$\sum E_{\text{in}} = \sum E_{\text{out}}. \tag{1}$$

3.1. The energy balance equation for the upper convective zone (UCZ)

The energy flows in terms of heat. Thus, the heat balance can be written as

$$Q_{(I,K+1)} = Q_{\text{solar}} + Q_{(I+1,K)} - Q_{(I,J,K)} - Q_{\text{wa}}, \tag{2}$$

where $Q_{(I,K+1)}$ is the total heat absorbed by the Ith layer at time $K+1$ (MJ), Q_{solar} is the net solar incidence reaching the Ith layer (MJ), $Q_{(I+1,K)}$ is the total heat transmitted from the subsequent layer $(I+1)$ (MJ), $Q_{(I,J,K)}$ is the total heat loss to the side walls of the pond (MJ), and Q_{wa} is the total heat lost to the surroundings from the upper layer (MJ).

So, the energy balance in differential form, based upon Eq. (2), for UCZ becomes

$$\begin{aligned}(X_1-\delta)\rho CA\frac{\partial T}{\partial t} &= \beta EA_{(\text{UCZ},I)}[1-(1-F)h_I(X_1-\delta)] \\ &\quad + kA\left.\frac{\partial T}{\partial x}\right|_{x=x_I} - A_{01}R_{\text{ps}}\left[(T_{I,K}) - T_{(I,J,K)}\right] \\ &\quad - U_{\text{wa}}A\left[T_{(I,K)} - T_{\text{a}}\right],\end{aligned} \tag{2a}$$

and in non-differential form it results in

$$\begin{aligned}(X_1-\delta)\frac{\rho CA}{\Delta t}\left[T_{(I,K+1)} - T_{(I,K)}\right] &= \beta EA_{(\text{UCZ},I)}[1-(1-F)h_I(X_1-\delta)] \\ &\quad + \frac{kA}{\Delta x_I}\left[T_{(I+1,K)} - T_{(I,K)}\right] - A_{01}R_{\text{ps}}\left[T_{(I,K)} - T_{(I,J,K)}\right] \\ &\quad - U_{\text{wa}}A\left[T_{(I,K)} - T_{\text{a}}\right],\end{aligned} \tag{2b}$$

and hence the temperature needed is extracted as follows:

$$T_{(I,K+1)} = T_{(I,K)} + \frac{\Delta t}{(X_1-\delta)\rho CA}\left\{\beta EA_{(\mathrm{UCZ},I)}[1-(1-F)h_I \times (X_1-\delta)] + \frac{kA}{\Delta x_I}\left[T_{(I+1,K)} - T_{(I,K)}\right] - A_{01}R_{\mathrm{ps}} \times \left[T_{(I,K)} - T_{(I,J,K)}\right] - U_{\mathrm{wa}}A\left[T_{(I,K)} - T_{\mathrm{a}}(n,t)\right]\right\}, \quad (2c)$$

where I varies from 1 to 2 and K from 1 to 24 h, respectively; X_1 is the total thickness of the UCZ; A_{01} is the surface area of the painted metal sheet on the side wall (m^2) and taken as ($8\times 0.05 = 0.4\ m^2$); δ is the thickness of the layer in the UCZ which absorbs the long-wave solar incident (m); E is the total solar incident reaching the pond surface (MJ), A is the upper surface area of the pond (m^2); ρ is the density of the layers in the UCZ (kg/m^3); C is the specific heat of the layers in the UCZ (MJ/kg °C); and k is the thermal conductivity of the layers in the UCZ (MJ/m °C h). These values are given in Table 1. Note that β is the fraction of the incident solar incident that actually enters the pond [11]:

$$\beta = 1 - 0.6\left[\frac{\sin(\theta_i-\theta_r)}{\sin(\theta_i+\theta_r)}\right]^2 - 0.4\left[\frac{\tan(\theta_i-\theta_r)}{\tan(\theta_i+\theta_r)}\right]^2, \quad (3)$$

and h_I is representing the ratio of the solar energy reaching depth in the layer I to the total solar incident falling on to the surface of the pond, which can be obtained from the following equation [9]:

$$h(X_1-\delta) = 0.727 - 0.056\ln\left[\frac{(X_1-\delta)}{\cos\theta_r}\right], \quad (4)$$

here R_{ps} is the thermal resistance of the painted metal sheet surrounding the first layer (MJ/m^2 °C h) which can be expressed as

$$R_{\mathrm{ps}} = \frac{k_p k_s}{S_p k_s + S_s k_p}, \quad (5)$$

where k_p and k_s are the thermal conductivities of the paint and iron-sheet (MJ/m °C h) and S_p and S_s are the corresponding thicknesses (m).

Also, F is the fraction of the incident solar energy absorbed by the pond's upper layer, and A_{UCZ} is the net upper surface area of the UCZ that receives the solar incident and is defined as

$$A_{(\mathrm{UCZ},I)} = L_W[L_L - (\delta + (I-1)\Delta x)\tan_r], \quad (6)$$

where θ_r the angle of the refraction of the solar beam (rad), Δx is the thickness of each layer in the UCZ (m) and taken as 0.005 m in the calculations, and L_W and L_L are the width and length of the pond (m). The last term in (Eq. (2c)) represents the heat loss to the surrounding air. Here, T_a stands for the air temperature at time t of nth day of a year [14]:

$$T_a(n,t) = 20 + 8\sin\left[\left(\frac{360}{365}\right)n - 103\right] + 5\sin\left[\left(\frac{360}{24}\right)t\right]. \quad (7)$$

For the second layer, e.g., $(I+1)$ in the UCZ, we use Eq. (2c) except that we replace U_{wa} and $T_a(n,t)$ with $\frac{kA}{\Delta x}$ and $T_{(I-1,J,K)}$.

3.2. The energy balance equation for the non-convective zone (NCZ)

Here the heat balance can be written as

$$Q_{(I,K+1)} = Q_{\mathrm{solar}} + Q_{(I+1,K)} - Q_{(I-1,K)} - Q_{(I,J,K)}, \quad (8)$$

where $Q_{(I-1,K)}$ is the total heat absorbed by the $(I-1)$th layer at time K (MJ).

Thus, the energy balance in differential form, based upon Eq. (8), for NCZ becomes

$$\rho CA\Delta x\frac{\partial T}{\partial t} = \beta EA_{(\mathrm{NCZ},I)}\left[(1-F)\left(h_{(I)}(x-\delta) - h_{(I+1)}(x+\Delta x-\delta)\right)\right] + kA\left.\frac{\partial T}{\partial x}\right|_{x=x_{I+1}} - kA\left.\frac{\partial T}{\partial x}\right|_{x=x_{I-1}} - A_{01}R_{\mathrm{ps}}\left[T_{(I,K)} - T_{(I,J,K)}\right], \quad (8a)$$

and in non-differential form it results in

$$\frac{\rho CA\Delta x}{\Delta t}\left[T_{(I,K+1)} - T_{(I,K)}\right] = \beta EA_{(\mathrm{NCZ},I)}\left[(1-F)\left(h_{(I)}(x-\delta) - h_{(I+1)}(x+\Delta x-\delta)\right)\right] + \frac{kA}{\Delta x}\left[T_{(I+1,K)} - T_{(I,K)}\right] - \frac{kA}{\Delta x}\left[T_{(I,K)} - T_{(I-1,K)}\right] - A_{01}R_{\mathrm{ps}}\left[T_{(I,K)} - T_{(I,J,K)}\right], \quad (8b)$$

and hence the layer temperature can be extracted in the following form:

$$T_{(I,K+1)} = T_{(I,K)} + \frac{\Delta t}{\rho CA\Delta x}\left\{\beta EA_{(\mathrm{NCZ},I)}(1-F)\left[h_{(I)}(x-\delta) - h_{(I+1)}(x+\Delta x-\delta)\right] + \frac{kA}{\Delta x}\left[T_{(I+1,K)} - T_{(I,K)}\right] - \frac{kA}{\Delta x}\left[T_{(I,K)} - T_{(I-1,K)}\right] - A_{01}R_{\mathrm{ps}}\left[T_{(I,K)} - T_{(I,J,K)}\right]\right\}, \quad (8c)$$

where I varies from 2 to 14.

We define the net upper surface area of the NCZ, A_{NCZ} as follows:

$$A_{(\mathrm{NCZ},I)} = L_W[L_L - (X_1 + (I-1)\Delta x)\tan\theta_r]. \quad (9)$$

3.3. The energy balance equation for the heat storage zone (HSZ)

For this zone, Eq. (8) is again representing the energy balance and used in the calculations. This means that the amount of heat absorbed by the NCZ is equal to the amount of heat coming from the storage zone. Here, the same iterative approach is used for the temperature distribution, which results in

$$\frac{\rho CA\Delta x}{\Delta t}\left[(T_{I,K+1})-T_{(I,K)}\right] = \beta EA_{(\mathrm{HSZ},I)}(1-F)\left[h_{(I)}(X-\delta)\right]+\frac{kA}{\Delta x}\left[T_{(I+1,K)}-T_{(I,K)}\right] - \frac{kA}{\Delta x}\left[T_{(I,K)}-T_{(I-1,K)}\right]-A_{01}R_{\mathrm{ps}}\left[T_{(I,K)}-T_{(I,J,K)}\right], \quad (10)$$

and the storage layer temperature is extracted from the above equation as follows:

$$T_{(I,K+1)} = T_{(I,K)}+\frac{\Delta t}{\Delta x\rho CA}\left\{\beta EA_{(\mathrm{HSZ},I)}(1-F)[h(x-\delta)] + \frac{kA}{\Delta x}\left[T_{(I+1,K)}-T_{(I,K)}\right]-\frac{kA}{\Delta x}\left[T_{(I,K)}-T_{(I-1,K)}\right] - A_{01}R_{\mathrm{ps}}\left[T_{(I,K)}-T_{(I,J,K)}\right]\right\}, \quad (11)$$

where I varies from 15 to 30.

Here, the net surface area of HSZ is equal to the net surface area of NCZ as $A_{\mathrm{HSZ}} = A_{\mathrm{NCZ}}$.

3.4. The energy balance equation for the insulated bottom wall (IBW)

The heat balance in this section becomes

$$Q_{(I,K+1)} = Q_{(I-1,K)} - Q_{(I+1,K)} - Q_{(I,J,K)}, \quad (12)$$

since Q_{solar} is not available in this layer and the direction of heat transfer is now opposite toward the ground as shown in Fig. 1. But the same iterative approach is used for the temperature distribution which results in the following based on Eq. (12):

$$\rho_{\mathrm{ins}}C_{\mathrm{ins}}\Delta x_{\mathrm{ins}}A\frac{\partial T}{\partial t} = AR_{\mathrm{ps}}\left[T_{(I-1,K)}-T_{(I,K)_{\mathrm{b}}}\right]-k_{\mathrm{ins}}A\left.\frac{\partial T}{\partial x}\right|_{x=x_{\mathrm{ins}}} - k_{\mathrm{ins}}A_{(J)}\left.\frac{\partial T}{\partial y}\right|_{y=y_{\mathrm{ins}}}. \quad (12a)$$

For the first layer (e.g., $I = 31$, $J = 1$) in the IBW,

$$\frac{\rho_{\mathrm{ins}}C_{\mathrm{ins}}\Delta x_{\mathrm{ins}}A}{\Delta t}\left[T_{(I,K+1)_{\mathrm{b}}}-T_{(I,K)_{\mathrm{b}}}\right] = AR_{\mathrm{ps}}\left[T_{(I-1,K)}-T_{(I,K)_{\mathrm{b}}}\right]-\frac{k_{\mathrm{ins}}A}{\Delta x_{\mathrm{ins}}}\left[T_{(I,K)_{\mathrm{b}}}-T_{(I+1,K)_{\mathrm{b}}}\right] - \frac{k_{\mathrm{ins}}A_{(J)}}{\Delta y}\left[T_{(I,K)_{\mathrm{b}}}-T_{(I,J,K)}\right], \quad (13)$$

and the insulated bottom wall temperature is extracted from the above equation as follows:

$$T_{(I,K+1)_{\mathrm{b}}} = T_{(I,K)_{\mathrm{b}}}+\frac{\Delta t}{\rho_{\mathrm{ins}}C_{\mathrm{ins}}\Delta x_{\mathrm{ins}}A}\left\{AR_{\mathrm{ps}}[T_{(I-1,K)}-T_{(I,K)_{\mathrm{b}}}] - \frac{k_{\mathrm{ins}}A}{\Delta x_{\mathrm{ins}}}\left[T_{(I,K)_{\mathrm{b}}}-T_{(I+1,K)_{\mathrm{b}}}\right]-\frac{k_{\mathrm{ins}}A_{01}}{\Delta y}\left[T_{(I,K)_{\mathrm{b}}}-T_{(I,J,K)}\right]\right\}, \quad (14)$$

where I varies from 31 to 35 and $\Delta x_{\mathrm{ins}} = \Delta y = 1\times10^{-2}$ m.

Note that for the layers in the wall (from 32 to 34) we employ $\frac{k_{\mathrm{ins}}}{\Delta x_{\mathrm{ins}}}$ instead of R_{ps}, and for the last layer ($I = 35$) we use $\frac{k_{\mathrm{ins}}}{\Delta x_{\mathrm{ins}}}$, h_α and $T_{\mathrm{a}}(n,t)$ to replace R_{ps}, $\frac{k_{\mathrm{ins}}}{\Delta x_{\mathrm{ins}}}$ and $T_{(I+1,K)_{\mathrm{b}}}$.

3.5. The energy balance equation for the insulated side wall (ISW)

In this zone, the heat transfer takes place in two directions (horizontally and vertically). In the analysis, the wall is divided into 35 layers (shown by I), same as the pond and 5 columns (shown by J). The heat balance equation for this wall becomes:

$$Q_{(I,J,K+1)} = Q_{(I,K)} + Q_{(I+1,J,K)} - Q_{(I,J+1,K)} - Q_{\mathrm{air}}, \quad (15)$$

where I and J values represent the later and column numbers as indicated in Fig. 1. $Q_{(I,J,K+1)}$ is the amount of heat absorbed by the cell defined as node (I,J)th; $Q_{(I,K)}$ is the amount of heat transfer to the cell node (I,J)th from the Ith layer (MJ); $Q_{(I+1,J,K)}$ is the amount of the heat transfer to (I,J)th from $(I+1)$th layer (MJ); $Q_{(I,J+1)}$ is the amount of heat transfer to $(I,J+1)$th from the (I,J) (MJ); and Q_{air} is amount of the heat loss to the surrounding air from the top.

Eq. (15) is written in the differential form as

$$V_{(J)}\rho_{\mathrm{ins}}C_{\mathrm{ins}}\frac{\partial T}{\partial t} = A_{(J)}R_{\mathrm{ps}}\left[T_{(I,K)}-T_{(I,J,K)}\right]+k_{\mathrm{ins}}A_{(J)\mathrm{down}}\left.\frac{\partial T}{\partial x}\right|_{x=x_{\mathrm{ins}}} + k_{\mathrm{ins}}A_{(J+1)}\left.\frac{\partial T}{\partial y}\right|_{y=y_{\mathrm{ins}}} - A_{(J)\mathrm{up}}h_\alpha\left[T_{(I,J,K)}-T_{\mathrm{a}}(n,t)\right]. \quad (15a)$$

Based upon Eq. (15), the temperature equation can be written in the following manner:

$$\frac{V_{(J)}\rho_{\mathrm{ins}}C_{\mathrm{ins}}}{\Delta t}\left[T_{(I,J,K+1)}-T_{(I,J,K)}\right] = A_{(J)}R_{\mathrm{ps}}\left[T_{(I,K)}-T_{(I,J,K)}\right]+\frac{k_{\mathrm{ins}}A_{(J)\mathrm{down}}}{\Delta x}\left[T_{(I+1,J,K)}-T_{(I,J,K)}\right] - \frac{k_{\mathrm{ins}}A_{(J+1)}}{\Delta y}\left[T_{(I,J,K)}-T_{(I,J+1,K)}\right]-A_{(J)\mathrm{up}}h_\alpha\left[T_{(I,J,K)}-T_{\mathrm{a}}(n,t)\right], \quad (15b)$$

and the wall temperature then becomes

$$T_{(I,J,K+1)} = T_{(I,J,K)}+\frac{\Delta t}{V_{(J)}\rho_{\mathrm{ins}}C_{\mathrm{ins}}}\left\{A_{(J)}R_{\mathrm{ps}}\left[T_{(I,K)}-T_{(I,J,K)}\right] + \frac{k_{\mathrm{ins}}A_{(J)\mathrm{down}}}{\Delta x}\left[T_{(I+1,J,K)}-T_{(I,J,K)}\right]-\frac{k_{\mathrm{ins}}A_{(J+1)}}{\Delta y} \times\left[T_{(I,J,K)}-T_{(I,J+1,K)}\right]-A_{(J)\mathrm{up}}h_\alpha\left[T_{(I,J,K)}-T_{\mathrm{a}}(n,t)\right]\right\}, \quad (15c)$$

where ρ_{ins}, C_{ins} and k_{ins} are density, specific heat and thermal conductivity of the insulating material within the wall as tabulated in Table 1. h_α is heat transfer coefficient, $V_{(J)}$ is the volume of the Jth rectangular ring (concentric node)

within the wall around the pond (m^3) and for the present work it is defined as

$$V_{(J)} = 0.00402 + 8(J-1)\Delta x\Delta y^2, \tag{16}$$

with $\Delta x = 0.05$ m and $\Delta y = 0.01$ m.

Here, A_J is the surface area between the two concentric nodes as represented with J and $J+1$ (m^2) and becomes

$$A_{(J)} = 0.4 + 8(J-1)\Delta x\Delta y. \tag{17}$$

On the other hand, $A_{(J)\text{up}}$ and $A_{(J)\text{down}}$ stand for the upper or lower (down) surface area of the Jth node, and are given by

$$A_{(J)\text{up}} = A_{(J)\text{down}} = 0.0804 + 8(J-1)\Delta y^2, \tag{18}$$

Note that $T_a(n,t)$ in Eqs. (15b) and (15c) is given by in Eq. (7).

We have to redefine some parameters in calculating the temperatures through Eq. (15c), as follows:

(i) For $I = 2$–30 and $J = 1$, we use $\frac{k_{\text{ins}}}{\Delta y}$ and $T_{(I-1,J,K)}$ instead of h_α and $T_a(n,t)$, respectively.
(ii) For $I = 1$ and $J = 2$–4, from now we employ $\frac{k_{\text{ins}}}{\Delta y}$ and $T_{(I,J-1,K)}$, instead of R_{ps} and $T_{(I,K)}$, respectively.
(iii) For $I = 1$ and $J = 5$, we replace R_{ps}, $T_{(I,K)}$, $\frac{k_{\text{ins}}A_{(J+1)}}{\Delta y}$ and $T_{(I,J+1,K)}$, with $\frac{k_{\text{ins}}}{\Delta y}$, $T_{(I,J-1,K)}$, $A_{(J+1)}h_\alpha$ and $T_a(n,t)$, respectively.
(iv) For $I = 2$–30, $J = 5$, we replace $A_{(J)}R_{\text{ps}}$, $T_{(I,K)}$, $\frac{k_{\text{ins}}A_{(J+1)}}{\Delta x}$, $T_{(I,J+1,K)}$, h_α and $T_a(n,t)$ with $\frac{k_{\text{ins}}A_{(J)}}{\Delta y}$, $T_{(I,J-1,K)}$, $A_{(J+1)}h_\alpha$, $T_a(n,t)$, $\frac{k_{\text{ins}}}{\Delta x}$ and $T_{(I-1,J,K)}$, respectively.
(v) For $I = 2$–30, $J = 2$–4, we replace $A_{(J)}R_{\text{ps}}$, $T_{(I,K)}$, h_α and $T_a(n,t)$ with $\frac{k_{\text{ins}}A_{(J)}}{\Delta y}$, $T_{(I,J-1,K)}$, $\frac{k_{\text{ins}}}{\Delta x}$ and $T_{(I-1,J,K)}$, respectively.
(vi) According Eq. (15b) (for $I = 31$–34, $J = 1$), we end up with the following equation for temperature distribution:

$$\begin{aligned} T_{(I,J,K+1)} &= T_{(I,J,K)} + \frac{\Delta t}{V_{(J)}\rho_{\text{ins}}C_{\text{ins}}}\left\{\frac{k_{\text{ins}}A_{(J)}}{\Delta y}\left[T_{(I,K)} - T_{(I,J,K)}\right]\right. \\ &\quad + \frac{k_{\text{ins}}A_{(J)\text{up}}}{\Delta x_{\text{ins}}}\left[T_{(I-1,J,K)} - T_{(I,J,K)}\right] \\ &\quad - \frac{k_{\text{ins}}A_{(J+1)}}{\Delta y}\left[T_{(I,J,K)} - T_{(I,J+1,K)}\right] \\ &\quad \left. - \frac{k_{\text{ins}}A_{(J)\text{down}}}{\Delta x_{\text{ins}}}\left[T_{(I,J,K)} - T_{(I+1,J,K)}\right]\right\}. \end{aligned} \tag{19}$$

(vii) In Eq. (19) (for $I = 31$–34, $J = 2$–4), we replace $T_{(I,K)}$ with $T_{(I,J-1,K)}$.
(viii) For $I = 31$–34, $J = 5$, we replace $T_{(I,K)}$, $T_{(I,\,J+1,\,K)}$, $\frac{k_{\text{ins}}A_{(J+1)}}{\Delta y}$ with $T_{(I,J-1,K)}$, $T_a(n,t)$, $h_\alpha A_{(J+1)}$.
(ix) For $I = 35$, $J = 5$, we replace $T_{(I,K)}$, $\frac{k_{\text{ins}}A_{(J+1)}}{\Delta y}$, $T_{(I,J+1,K)}$, $\frac{k_{\text{ins}}A_{(J)\text{down}}}{\Delta x_{\text{ins}}}$ with $T_{(I,J-1,K)}$, $h_\alpha A_{(J+1)}$, $T_a(n,t)$, and $h_\alpha A_{(J)\text{down}}$.
(x) For $I = 35$, $J = 1$, we replace $\frac{k_{\text{ins}}A_{(J)\text{down}}}{\Delta x_{\text{ins}}}$, $T_{(I+1,J,K)}$ with $A_{(J)\text{down}}$ h_α, $T_a(n,t)$, and finally,
(xi) For $I = 35$, $J = 2$–4, we replace $T_{(I,K)}$, $\frac{k_{\text{ins}}A_{(J)\text{down}}}{\Delta x_{\text{ins}}}$, $T_{(I+1,J,K)}$ with $T_{(I,J-1,K)}$, $h_\alpha A_{(J)\text{down}}$ and $T_a(n,t)$, respectively.

The above 2-D modeling is employed to estimate temperature distributions in the pond and in its wall at any time and point with time of the day.

4. Results and discussion

Table 1 lists the thermophysical properties of substances and materials in the pond in terms of density, thermal conductivity and specific heats, respectively. Fig. 2 shows the variations of the experimental salty water densities with the height from the bottom of the pond in various months (e.g., January, May and August). Here, some slight differences are observed between the density variation measured for these three different months, due essentially to increase of the inner zone temperature and to diffusion of the salt molecules. The primary reason for differences might be the increase in temperature in summer. This change mostly originates from the thermophysical property of the salty water. The reason for the fluctuations of the saline density in the upper layers (UCZ and IZ) is the increase in saline density of these zones due to the evaporation of the water at the upper region. These changes can be eliminated by continuously adding fresh water to the top of the pond. Due to the cancellation of one of the salt gradient protection systems for cleaning purpose in a month, significant changes occurred in the non-convective region and upper convective region.

The modeling presented above is used to calculate the temperature distributions in the three zones of the pond, (namely upper convective zone (UCZ), non-convective zone (NCZ) and heat storage zone (HSZ)), in the insulated bottom wall (IBW), and in the insulated side wall (ISW). These estimated temperature distributions are then compared with the experimental temperature measurements taken from the pond. Fig. 3 shows the comparisons of both theoretical temperature variations and average experimental temperature distributions measured inside pond during day times in the months of January, May and August. These experimental temperatures were in fact measured on hourly basis between the following times, such as 8:00 am to 5:00 pm in January and 6:00 am to 7:00 pm in both May and August, with an accuracy of ±0.1 °C. For the calculations, a custom-designed computer program was constructed, with our own code in Pascal programming language, rather than a commercial software package, to consider all remedies for more accurate solution. As clearly seen in the figure, there is a very good agreement between experimental data and theoretical calculation results and that the average differences are 22.7% for January, 12.1% for May and 7.9% for August, respectively. From the temperature point of view the maximum differences between experimental data and theoretical calculations for the HSZ are found to be 1.5 °C for January, 3 °C for May and 2.8 °C for August, respectively. As also seen in the figure, the experimental and theoretical distributions follow the same trend. Furthermore, these distributions roughly

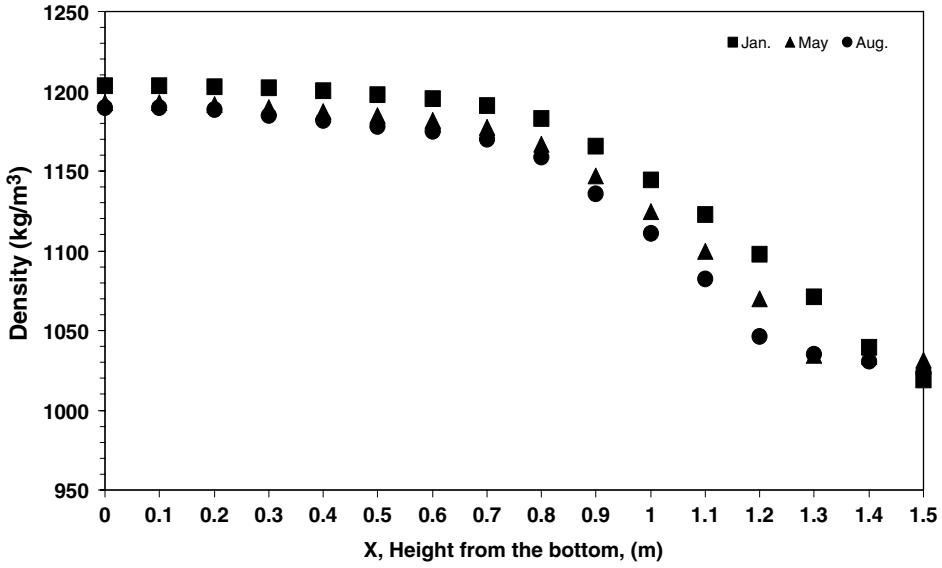

Fig. 2. The inner zones' salt density distribution of the solar pond.

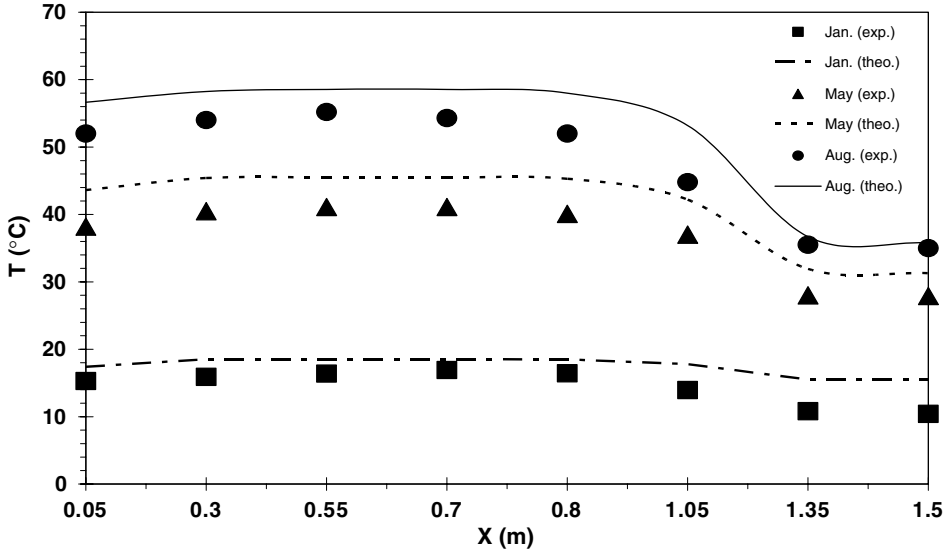

Fig. 3. The average experimental and theoretical temperature distributions inside the pond during daytimes for some selected months.

remain constant in the HSZ (from the bottom to 0.8 m high) and decrease exponentially in the NCZ (from 0.8 to 1.35 m high) and again remain almost constant in the UCZ (from 1.35 m to the surface of the pond where the surface temperature approaches the ambient temperature). In the winter time (e.g., January) the temperature profiles do not change drastically and end up with a little change due to the large heat losses. This is because of the fact that the NCZ is normally expected to be thicker. In practice the optimum thickness of this zone is chosen as 1.3 m [14].

We now repeat the above calculations for the nighttimes (times excluding daytimes) and compare both experimental and theoretical temperature distributions for the pond in the above listed months (e.g., January, May and August) in Fig. 4. The experimental temperatures were in fact measured on hourly basis during nighttimes. Here, we observe better agreement between experimental and theoretical temperature values, resulting in average differences as 9.4% for January, 3.8% for May and 4.3% for August, respectively. The temperature profiles follow a trend similar to the daytime variations. It is apparent that at nighttime there are larger heat losses, referring to discharging process due to the inexistence of the solar irradiation. In terms of temperatures the maximum differences between experimental data and theoretical calculations for the HSZ are found to be 1.5 °C for January, 1.0 °C for May and 1.2 °C for August, respectively.

In addition to the above comparisons between both experimental and theoretical temperature distributions in the pond, we measured the temperatures in the insulated

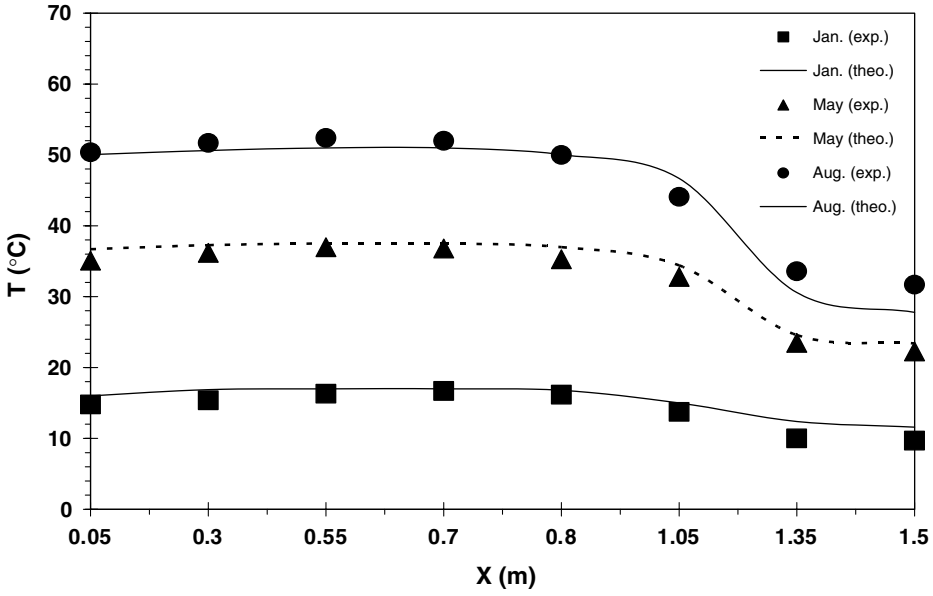

Fig. 4. The average experimental and theoretical temperature distributions inside the pond versus height (from bottom to the top) during nighttimes for some selected months.

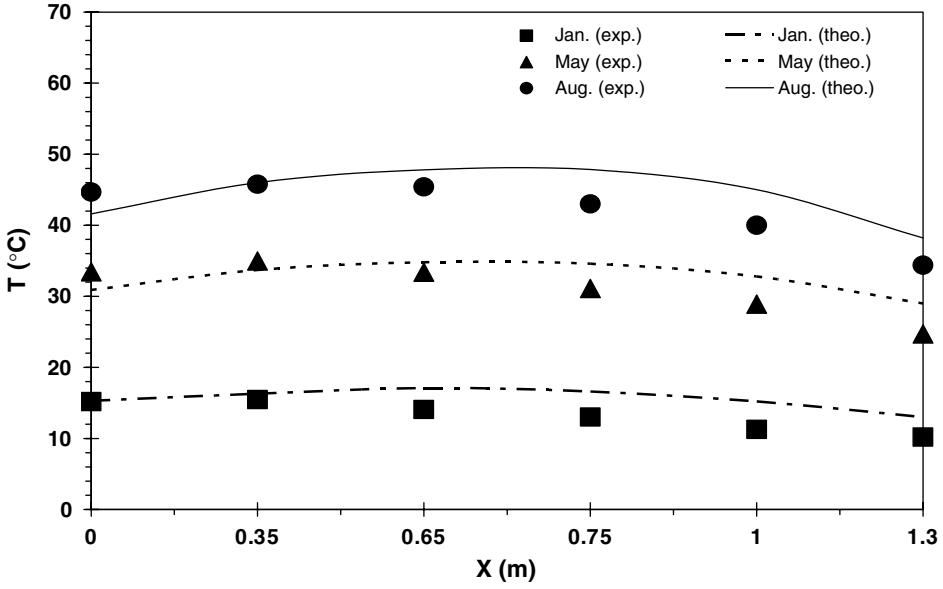

Fig. 5. The average experimental and theoretical temperature distributions in the side wall versus height (from bottom to the top) during daytimes for some selected months.

Table 2
Some example values of experimental and theoretical daytime and nighttime temperatures at the bottom wall of the solar pond and the percent differences

Δx_i ($\times 10^{-2}$ m)		Daytime			Nighttime		
		T_{exp} (°C)	T_{theo} (°C)	Difference (%)	T_{exp} (°C)	T_{theo} (°C)	Difference (%)
1.5	January	15.63	16.00	2.37	15.20	15.55	2.30
	May	33.56	31.62	3.16	32.35	33.25	2.78
	August	44.67	45.88	2.71	43.20	44.30	2.55
4.5	January	15.08	15.62	2.23	14.54	14.88	2.24
	May	27.40	28.00	2.19	26.25	27.00	2.86
	August	36.60	37.22	1.97	36.31	37.10	2.77

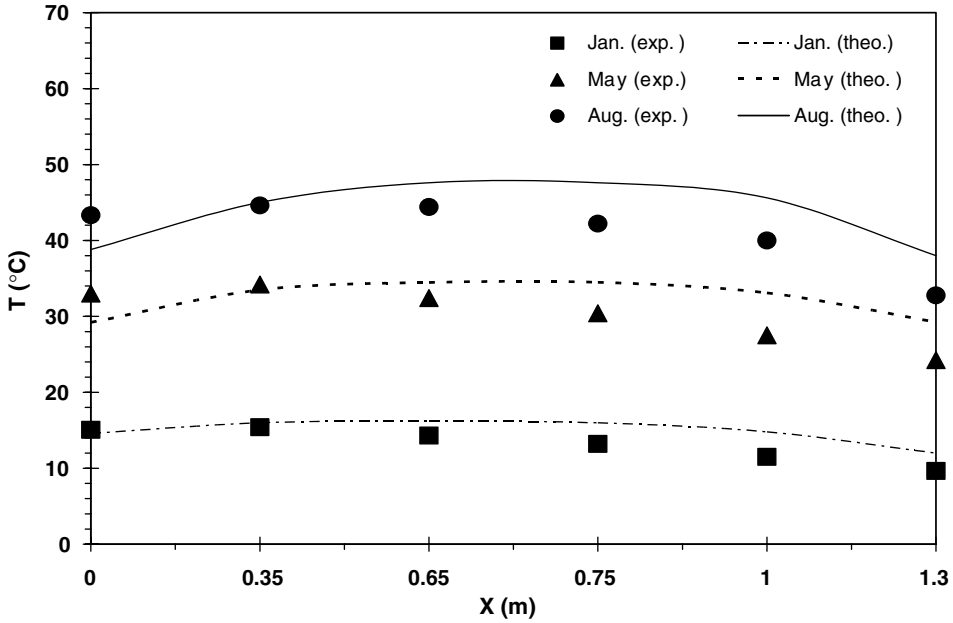

Fig. 6. The average experimental and theoretical temperature distributions in the side wall versus height (from bottom to the top) during nighttimes for some selected months.

part (with glass-wool) at the bottom of the pond underneath the iron sheet at two locations 1.5 and 4.5 cm from the sheet and calculated the temperatures as well. A comparison of these temperatures is given is Table 2 for daytimes and nighttimes, with a considerable high agreement (with an average difference of 2.58%).

Figs. 5 and 6 exhibit the comparisons of both theoretical temperature variations and average experimental temperature distributions measured on hourly basis in the side wall of the pond vertically during daytimes and nighttimes in the months of January, May and August. It is apparent in the figures that there is a very good agreement between experimental data and theoretical calculation results and that the average differences for daytimes and nighttimes are 17.9% and 14.5% for January, 7.9% and 9.9% for May and 8.9% and 7.5% for August, respectively. The profiles in both figures follow the same trend and concave in a way that the temperature is approximately maximum in the middle of HSZ as expected. The reason is that there are heat losses from the surface and bottom of the pond.

Consequently, Fig. 7 presents a comparison of both experimental and theoretical temperature variations in the middle of the HSZ versus time of the day (hourly basis), e.g., on 15th of January, May and August. As seen,

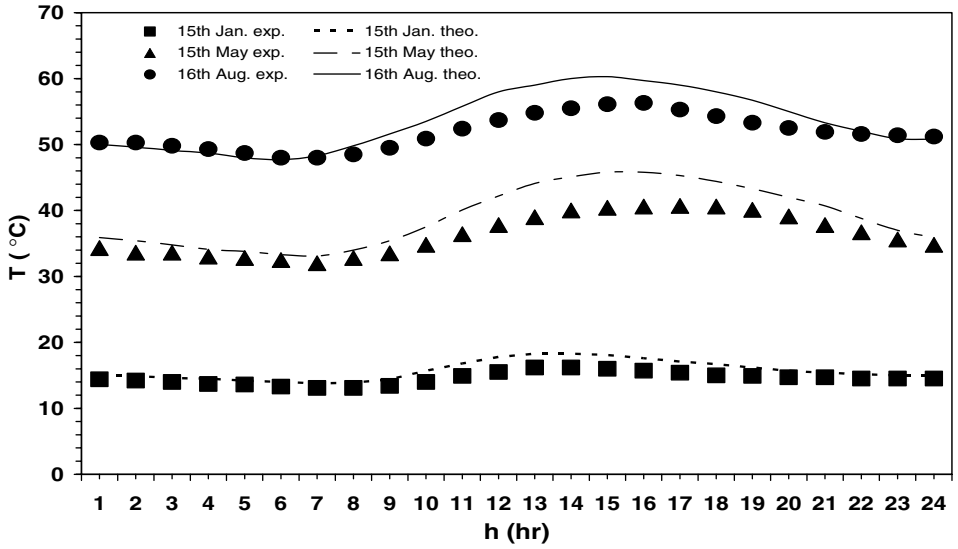

Fig. 7. Variation of hourly experimental and theoretical temperature distributions in the middle of the HSZ during a whole day in some selected days.

depending on the solar energy stored the profiles fluctuate and the smallest fluctuation takes place on 15th of January. As clearly seen in the figure, there is a considerable high agreement between the experimental data and theoretical calculation results and that the average differences are 8.0% for January, 7.2% for May and 3.8% for August, respectively. For the temperatures the maximum differences between experimental data and theoretical calculations for the HSZ are found to be 3.0 °C for January, 7.0 °C for May and 6.0 °C for August, respectively.

5. Conclusions

This paper deals with an experimental and theoretical study of temperature distributions in an insulated solar pond, particularly during daytimes and nighttimes. Experimental and theoretical temperature distributions calculated through the present model are compared for various cases, such as inside the pond, underneath the pond and in the side wall and a good agreement is found. There is a large amount of heat losses between daytimes and nighttimes, depending upon the temperature difference, and these present a significant potential for energy savings and storage.

Acknowledgements

The authors acknowledge the support provided by Cukurova University in Turkey, and University of Ontario Institute of Technology and the Natural Sciences and Engineering Research Council of Canada in Canada.

References

[1] I. Dincer, M.A. Rosen, Thermal Energy Storage Systems and Applications, Wiley, New York, 2003.
[2] A. Akbarzadeh, G. Ahmadi, Computer simulation of performance of a solar pond in southern part of Iran, Solar Energy 24 (1980) 143–151.
[3] F.B. Alagao, A. Akbarzadeh, P.W. Johnson, The design, construction and initial operation of a closed-cycle, salt-gradient solar pond, Solar Energy 53 (4) (1994) 343–351.
[4] T.A. Newell, R.G. Cowie, J.M. Upper, M.K. Smith, G.L. Cler, Construction and operation activities at the University of Illinois salt gradient solar pond, Solar Energy 45 (4) (1990) 231–239.
[5] R.S. Beniwal, R. Singh, N.S. Saxena, R.C. Bhandari, Thermal behaviour of salt gradient solar ponds, J. Phys. D: Appl. Phys. 20 (1987) 1067–1071.
[6] M.R. Jaefarzadeh, Thermal behavior of a small salinity-gradient solar pond with wall shading effect, Solar Energy 77 (2004) 281–290.
[7] M.R.I. Ramadan, A.A. El-Sebaii, S. Aboul-Enein, A.M. Khallaf, Experimental testing of a shallow solar pond with continuous heat extraction, Energy Build. 36 (9) (2004) 955–964.
[8] A.A. Badran, B.A. Jubran, E.M. Qasem, M.A. Hamdan, Numerical model for the behaviour of a salt-gradient solar pond greenhouse-heating system, Appl. Energy 58 (1) (1997) 57–72.
[9] H.C. Bryant, I. Colbeck, A solar pond for London, Solar Energy 19 (1977) 321.
[10] A. Celestino, E. Leonardi, A one-dimensional numerical study of the salt diffusion in a salinity-gradient solar pond, Int. J. Heat Mass Transfer 47 (1) (2004) 1–10.
[11] M.N.A. Hawlader, The influence of the extinction coefficient on the effectiveness of solar ponds, Solar Energy 25 (1980) 461–464.
[12] J.R. Hull, Computer simulation of solar pond thermal behavior, Solar Energy 25 (1980) 33–40.
[13] N.D. Kaushika, M.S. Sharma, Numerical model of a solar pond, Energy Convers. Manage. 25 (4) (1985) 459–461.
[14] R. Kayalı, S. Bozdemir, K. Kıymaç, A rectangular solar pond model incorporating empirical functions for air and soil temperatures, Solar Energy 63 (1998) 345–353.
[15] Y. Keren, H. Rubin, J. Atkinson, M. Priven, G.A. Bemporad, Theoretical and experimental comparison of conventional and advanced solar pond performance, Solar Energy 51 (4) (1993) 255–270.
[16] H. Kurt, F. Halici, A.K. Binark, Solar pond conception-experimental and theoretical studies, Energy Convers. Manage. 41 (9) (2000) 939.
[17] K.A. Meyer, A numerical model for describing the layer behaviour in salt-gradient solar ponds, ASME—J. Solar Energy Eng. 105 (1983) 341–347.
[18] M. Ouni, A. Guizani, H. Lu, A. Belghith, Simulation of the control of a salt gradient solar pond in the south of Tunisia, Solar Energy 75 (2) (2003) 95–101.
[19] M. Karakilcik, Determination of the performance of an insulated prototype solar pond, Ph.D. Thesis, Cukurova University, Adana, Turkey, 1998 (in Turkish).